Science of the Total Environment 970 (2025) 178970

Contents lists available at ScienceDirect

Science of the Total Environment

journal homepage: www.elsevier.com/locate/scitotenv

# Naturally occurring asbestos in Southern Italy: Geological and mineralogical investigation of fibrous antigorite from Calabrian serpentinites in view of its hazard assessment

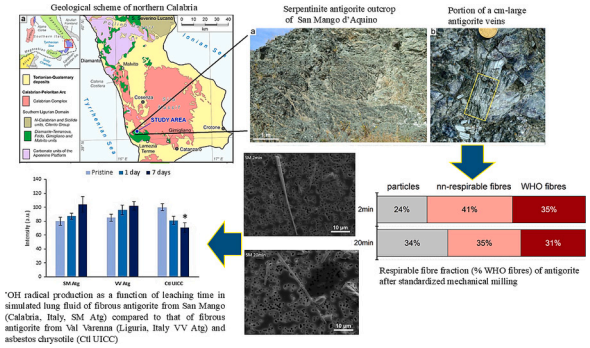
J.R. Petriglieri [a,b], G. Capitani [c], P. Ballirano [d,e], L. Barale [a,f], F. Piana [a,f], M. Tomatis [a,g], M.C. Di Carlo [d], F. Gianchiglia [d], A. Campopiano [h], A. Olori [h], M.R. Bruno [i], M.R. Montereali [j], E. Nardi [k], M. Fantauzzi [l], A. Rossi [l], H. Skogby [m], E. Belluso [a,b], F. Turci [a,n,*], A. Pacella [d,**]

[a] "G. Scansetti" Interdepartmental Centre for Studies on Asbestos and Other Toxic Particulates, University of Torino, Via Pietro Giuria 9, I-10125 Torino, Italy
[b] Department of Earth Sciences, University of Torino, Via Valperga Caluso 35, I-10125 Torino, Italy
[c] Department of Earth & Environmental Sciences, University of Milano Bicocca, School of Sciences, Piazza della Scienza 4, Milan 20126, Italy
[d] Department of Earth Sciences, Sapienza University of Rome, Piazzale Aldo Moro 5, I-00185 Rome, Italy
[e] Rectoral Laboratory Fibres and Inorganic Particulate, Sapienza University of Rome, Piazzale Aldo Moro 5, I-00185 Rome, Italy
[f] Institute of Geosciences and Earth Resources, National Research Council (CNR) of Italy, Torino, Italy
[g] Department of Veterinary Sciences, L.go Braccini, 2, 10095 Grugliasco (TO), Italy
[h] National Institute for Insurance against Accidents at Work (INAIL), Department of Medicine, Epidemiology, Occupational and Environmental Hygiene, via Fontana Candida 1, 00078, Monte Porzio Catone, Rome, Italy
[i] Department of Medicine, Epidemiology, Occupational and Environmental Hygiene, National Institute for Insurance against Accidents at Work (INAIL), Lamezia Terme, Italy
[j] Italian National Agency for New Technologies, ENEA, Casaccia Research Centre, via Anguillarese 301, I-00123, S. Maria di Galeria, Roma, Italy
[k] Institute for Environmental Protection and Research, ISPRA, via Vitaliano Brancati 48, 00144 Roma, Italy
[l] Department of Chemical and Geological Sciences, INSTM Research Unit, University of Cagliari, I-09042, Monserrato, Cagliari, Italy
[m] Swedish Museum of Natural History, Department of Geosciences, Box 50007, SE-104 05 Stockholm, Sweden
[n] Department of Chemistry, University of Torino, Via Pietro Giuria 7, I-10125 Torino, Italy

## HIGHLIGHTS

- A study on an occurrence of antigorite from Southern Apennines (Italy) evaluated its asbestos-like characteristics.
- Field, petrographic, minero-chemical, and morphometric parameters relevant to toxicity were assessed on the antigorite vein.
- Antigorite exhibits asbestos-like features, posing a potential environmental hazard that required further assessment.
- The San Mango D'Aquino site and Gimigliano-Monte Reventino serpentinites are a potential source of environmental hazard.

## GRAPHICAL ABSTRACT




* Correspondence to: F. Turci, "G. Scansetti" Interdepartmental Centre for Studies on Asbestos and Other Toxic Particulates, University of Torino, Via Pietro Giuria 9, I-10125 Torino, Italy.
** Corresponding author.
*E-mail addresses:* francesco.turci@unito.it (F. Turci), alessandro.pacella@uniroma1.it (A. Pacella).

https://doi.org/10.1016/j.scitotenv.2025.178970
Received 22 December 2024; Received in revised form 5 February 2025; Accepted 23 February 2025
Available online 3 March 2025
0048-9697/© 2025 The Authors. Published by Elsevier B.V. This is an open access article under the CC BY license (http://creativecommons.org/licenses/by/4.0/).

ARTICLE INFO

Editor: Pavlos Kassomenos

*Keywords:*
Fibrous antigorite
Naturally occurring asbestos NOA
Mineralogical investigation
Hazard assessment
Bio-durability
Surface chemical reactivity

ABSTRACT

In the last few decades, non-occupational asbestos-related diseases have been documented in populations living near naturally occurring asbestos (NOA) sites, including regions in Greece, Cyprus, China, New Caledonia, Turkey, and Italy. This highlights the critical need to assess geological and environmental hazards associated with NOA. Fibrous antigorite, among the >400 naturally occurring fibrous minerals, has emerged as a potential health and environmental hazard. This work examines the morphometrical, mineralogical and surface properties of a fibrous antigorite vein from a serpentinite body at San Mango D'Aquino (Calabria, Italy), relevant to assessing its potential toxicity. The geological site, described through field and petrographic analyses, was selected as representative of serpentinites outcropping over a large area in central Calabria. Results on the morphometric variation induced by a standardized mechanical stress, mineral solubility, and surface chemical reactivity indicated that: i) the fibrous morphology, expressed as % of WHO (World Health Organization) fibres, was largely preserved and consistent with asbestos standards; ii) antigorite fibres have a durability higher than chrysotile and close to a previously characterized fibrous antigorite from Val Varenna, Italy; iii) fibres showed a remarkable redox reactivity, even higher than chrysotile, suggesting that they may promote particle-derived radical imbalance in vitro and in vivo. Our findings revealed that the antigorite fibres from San Mango possess several critical properties commonly associated with asbestos toxicity. On this basis, we identify the NOA site of San Mango as a potential emission source of hazardous antigorite fibres, with significant environmental and public health implications for the surrounding communities.

## 1. Introduction

Naturally occurring asbestos (NOA) is a term for asbestos and asbestos-like minerals in their natural state, i.e., occurring as a natural constituent of rocks and soils due to geological processes (Harper, 2008; Lee et al., 2008). The NOA sites are widespread worldwide: large NOA bearing outcrops were reported in Canada, Russia, USA, India, China, Italy, South Africa, Australia, Greece, Cyprus and several other countries (Ross and Nolan, 2003; Virta, 2006; Gualtieri, 2020).

Human activities (mining, driving, cycling, agriculture, etc.) and/or natural weathering processes may disturb the NOA outcrops and induce the dispersion of the fibres into the environment (Lee et al., 2008; Koumantakis et al., 2009; Turci et al., 2016).

In the last few decades, non-occupational asbestos-related diseases have been documented among populations living near NOA deposits around the world, including in Greece, Cyprus, China, New Caledonia, Turkey, and Italy (Luo et al., 2003; Carbone et al., 2007; Constantopoulos, 2008; Bayram and Bakan, 2014; Bruno et al., 2014; Metintas et al., 2024).

Accordingly, these findings have prompted an intensified focus on non-occupational exposure to NOA aimed at investigating the potential health risks in the population that is resident in the proximity of NOA-rich outcrops (Baumann et al., 2011; Gualtieri et al., 2014; Vignaroli et al., 2014). Today, asbestos, and >400 mineral species with fibrous morphology are known in nature (Gualtieri, 2017; Baumann, 2024). Safety regulations do not generally include asbestos-like minerals and elongated mineral particles (EMP, NIOSH, 2011 definition) that might share asbestos mineral-chemical and toxicological properties (Gualtieri, 2020).

Fibre morphology affects deposition, translocation into the lung's deep part, and fibre clearance (Gualtieri, 2023). On this basis, several studies have addressed the dimensional characteristics of fibres to assess their toxicity and carcinogenicity (Stanton et al., 1981; Berman and Crump, 2008; Lippmann, 2009; Asgharian et al., 2018; Di Giuseppe et al., 2021; Wylie and Korchevskiy, 2023). Today, it is broadly accepted that longer and thinner fibres are the most carcinogenic. It should be noted that the term "EMP" does not indicate a mineral fibre that poses a higher risk for asbestos-related diseases. Therefore, the use of aspect ratio alone to define particle hazard should be avoided in EMP risk assessment (Weill, 2018). Recently, the physicochemical and functional properties of EMP that might have a relevance for mineral fibres toxicity have been described in terms of: i) bio-persistence and ii) surface reactivity (Oberdörster and Graham, 2018). Bio-persistence refers to the extent to which a fibre resists chemical, physical, and other physiological clearance mechanisms (Utembe et al., 2015). Bio-persistence is strongly affected by fibre solubility, which in turn is regulated by fibre crystal chemistry, and specific surface area. Solubility is commonly measured in terms of dissolution rate in several simulating body fluids (SBF). Surface reactivity refers to the ability of a mineral surface to alter functional biomolecules, in general, via oxidative reactions. One of the most critical forms of surface reactivity is the capacity to catalyse the generation of reactive oxygen species (ROS) in biological media (Oberdörster and Graham, 2018) that, together with cell-generated ROS (Kamp and Weitzman, 1999), contribute to the onset of oxidative stress. Transition metal ions, specifically surface-exposed iron ions, are well-known surface reactive sites that play a primary role in the fibre-induced production of ROS. ROS may overcome the cellular antioxidant defences and induce a sustained inflammatory response, leading to the onset of fibrosis and carcinogenicity (Cox et al., 2023 and references therein).

Among the naturally occurring mineral fibres, fibrous antigorite has emerged as a subject of growing interest due to its similarity with chrysotile (Cardile et al., 2007; Baumann et al., 2011; Baumann, 2012; Fitzgerald and Harty, 2014; Gazzano et al., 2023). Several publications have described the occurrence of fibrous antigorite in serpentinite rocks and soils worldwide (e.g. Anthony et al., 2001; Keeling et al., 2006; Groppo and Compagnoni, 2007; Bloise et al., 2014; Cluzel et al., 2020; Baumann, 2024).

Antigorite, lizardite, and chrysotile are polymorphs of the serpentine group, each with its unique crystalline structure. While they share the same ideal chemical formula [$Mg_3Si_2O_5(OH)_4$], their structure significantly differs. Antigorite shows an alternating-wave structure with continuous octahedral sheet and tilted $SiO_4$ tetrahedra that switch their orientation every half wavelength (Capitani and Mellini, 2004). In contrast, lizardite has a planar structure based on flat 1:1 layers (Mellini and Viti, 1994), and chrysotile has a cylindrical structure due to curled 1:1 layers (Wicks and O'Hanley, 1988).

High incidences of malignant mesothelioma associated with exposure to serpentinite outcrops rich in chrysotile and fibrous antigorite have been observed in New Caledonia (Baumann et al., 2011). Moreover, Baumann and Ambrosi (2013) suggested that exposure to fibrous antigorite might be related to the onset of asbestos-induced lung cancers and that soils containing fibrous antigorite might contribute to the overall risk faced by the Caledonian population when the fibres are released into the air by weathering or by human activities. Fibrous antigorite was reported to occur over a large part of the Caledonian island, and the Government of New Caledonia classified antigorite as asbestos, on a precautionary basis (Deliberation N. 82 du 25 aout, 2010).

It must be pointed out that, the Caledonian precautionary principle makes no distinction between lamellar and fibrous antigorite. However, it was evidenced a high variability of antigorite toxicity in vitro, depending on shape, mineral chemistry, and surface reactivity (Petriglieri et al., 2020; Gazzano et al., 2023).

In this context, the development of reliable methodologies for assessing the NOA hazard from different outcrops is of paramount importance. These methodologies are crucial for environmental protection agencies in their effort to protect the environment and the general population potentially exposed to NOA (Harper, 2008; Turci et al., 2016; Bloise et al., 2016, 2017). In a recent study, we employed a multidisciplinary approach encompassing geology, mineralogy, chemistry, and toxicology, to investigate antigorite at a specific NOA site in Varenna Valley near Genoa (Liguria, Italy). This site corresponds to a large serpentinite body cut by antigorite veins in the metaophiolites belonging to the Mesozoic Ligurian oceanic domain presently involved in the Ligurian Alps metamorphic complex (Petriglieri et al., 2023). Antigorite from one representative vein was characterized for: i) fibre morphology under a standardized mechanical stress, ii) mineral solubility, and iii) surface chemical reactivity. The results revealed the asbestos-like properties of the antigorite mineral in the Varenna Valley outcrop, prompting us to extend and test the approach on other fibrous minerals and NOA sites with potential hazards.

The protocol from Petriglieri et al. (2023) is here applied to investigate for the first time the occurrence and the potential toxic properties of a pure antigorite vein from a serpentinite body cropping out in San Mango D'Aquino (Calabria, Italy) and belonging to the southern part of the same Mesozoic Ligurian domain, presently involved in the Southern Apennines tectonic belt. The San Mango d'Aquino outcrop was selected as a representative site for the serpentinites cropping out over a large area in central Calabria, which shared a common geological evolution and thus have a potential to host fibrous minerals with similar characteristics. Results of the field analysis, the petrographic characterization of the rocks samples, and the investigation of asbestos-like properties (i.e., morphology, biodurability, and chemical reactivity) of antigorite fibres are discussed in comparison with those previously obtained for the site in Varenna Valley and standard reference asbestos. The investigation was eventually designed to define whether the San Mango D'Aquino site might be considered a source of emission of asbestos-like antigorite fibres, with relevant implications for the environment and nearby resident population.

## 2. Materials and methodology

### 2.1. Samples

The fibrous antigorite sample was collected from a vein hosted in a serpentinite body of the Gimigliano-Mount Reventino Unit, in San Mango D'Aquino (Calabria, Southern Italy). Following Petriglieri et al. (2023), a preliminary SEM morphological check was made on samples from different veins hosted in this outcrop to select the vein with the more pronounced fibrous habit. The specific surface area (SSA) of antigorite fibres (4.0 $m^2/g$) prepared for dissolution and surface reactivity tests was determined by Kr adsorption at 77 K, adopting the BET method (Brunauer et al., 1938) and using an automatic gas-volumetric apparatus (ASAP 2020, Micromeritics, USA).

Results of the morphological investigation were compared to those previously obtained by Petriglieri et al. (2023) on a fibrous antigorite sample from Varenna Valley (Genoa, NW Italy), on UICC (Union Internationale Contre le Cancer) crocidolite and chrysotile standard asbestos samples. Moreover, antigorite from Varenna Valley (SSA of 5.7 $m^2/g$) and UICC chrysotile (SSA of 27 $m^2/g$) were used for comparison in other to evaluate both fibre durability and surface reactivity of San Mango antigorite.

### 2.2. Sample preparation

Sample collection followed the protocols described by Petriglieri et al. (2023). Vein sample was collected by hand-picking with stainless steel tweezers after carefully removing the potentially altered superficial layer with the pointed tip of a pick hammer. Antigorite fragment veins were prior gently reduced in size and sieved to obtain a fraction <2 mm. This fraction was ground using two different methods: i) for the morphological assessment and ii) for the dissolution and surface reactivity tests.

Sample preparation i): the <2 mm fraction (1.8 g) was dry ground in a ball mixer mill (Retsch MM200) for 2, 5, 10, and 20 min at 27 Hz using an agate jar (15 mL) with 4 agate balls (5 mm diameter). Agate jars were used to prevent cross contamination by metals. After grinding, the powder sample was sieved at 300 μm.

Sample preparation ii): The <2 mm fraction (5.5 g) was wet grounded in a planetary ball mill (Fritsch P6) for 5 min at 450 rpm using a zirconium oxide jar (45 mL) with 4 g of zirconium oxide balls (5 mm diameter). A zirconium oxide jar was used to prevent cross-contamination by metals. After grinding, powder sample was washed in ultrapure water by centrifugation at 8000 rpm for 20 min, sieved at 100 μm, and dried at low temperature (60 °C).

### 2.3. Morphological and mineralogical characterization

#### 2.3.1. Flow Particle Image Analysis (FPIA)

Particle morphology and particle size distribution of antigorite in the range 0.8–300 μm were obtained by automatic image analysis using a Flow Particle Image Analysis (FPIA) Sysmex FPIA-3000 apparatus (Malvern Instruments). Antigorite powders (see sample preparation, Par 2.2i) were dispersed in ultrapure water (0.5 mg/mL) and sonicated at 10 W for 30 s. Each suspension was gone through a cell where pictures of particles were acquired using stroboscopic illumination and a CCD camera (20× magnification lens). More than 2000 particles were counted and measured for each specimen.

#### 2.3.2. X-ray powder diffraction (XRPD)

XRPD analysis was performed using a Bruker AXS D8 Advance diffractometer (Bruker AXS, Karlsruhe, Germany) operating in θ/θ transmission mode. The instrument is equipped with incident-beam focusing Göbel mirrors and a PSD Våntec-1. Data collection was made at 40 kV and 40 mA, using CuKα radiation in the 5–145° 2θ angular range, 0.0218° 2θ step-size, and 10 s of counting time.

#### 2.3.3. Scanning and transmission electron microscopies

Secondary Electron Images (SEI) were acquired at various magnifications using a Scanning Electron Microscope (SEM) ZEISS EVO50 XVP equipped with an X-Stream OXFORD EDS (accelerating voltages, commonly 3–10 kV).

Transmission electron microscopy (TEM) observations were performed with a JEOL JEM 2100P at the Platform of Microscopy of the University of Milano-Bicocca. The instrument is equipped with an Oxford UltimMax energy dispersive spectrometer (EDS) for elemental analysis and a Gatan Rio CMOS camera for image acquisition. Contrast in high resolution TEM images (HRTEM) was improved by the HRTEM filter (Mitchell, 2007) in the Digital Micrograph (Gatan) program. EDS analyses were acquired with Aztec (Oxford) software and quantified within the Cliff and Lorimer approximation (Cliff and Lorimer, 1975) using standards of known composition (Conconi et al., 2023). TEM samples were prepared by ion milling 3 mm wide disks obtained from a petrographic thin section using a Gatan precision ion polishing system (PIPS) at the Department of Physical Sciences, Earth and Environment of the University of Siena.

#### 2.3.4. Electron Microprobe Analysis (EMPA)

The micro-chemical analysis of the antigorite fibres was performed

using a Cameca SX-50 electron microprobe equipped with five wavelength-dispersive spectrometers, operating under the following conditions: excitation voltage 15 kV, specimen current 15 nA, beam diameter 10 μm, 20 s count time (peak), 10 s count time (background). The following standards were used: wollastonite (Si Kα, Ca Kα), rutile (Ti Kα), corundum (Al Kα), magnetite (Fe Kα), metallic Mn (Mn Kα), periclase (Mg Kα), orthoclase (K Kα), jadeite (Na Kα), metallic Cr (Cr Kα), fluorophlogopite (F Kα), and sylvite (Cl Kα).

#### 2.3.5. Mössbauer spectroscopy

Mössbauer data were collected at room temperature using a conventional spectrometer system operated in constant-acceleration mode. Approximately 70 mg of antigorite fibres were gently ground in an agate mortar with acetone and mixed with 100 mg of powdered acrylic resin to avoid (or at least reduce) preferred orientations. The mixture was pressed to a 12 mm diameter disc under mild heating. The spectrum was collected at room temperature using a standard $^{57}$Co source in a Rh matrix (nominal activity of 50 mCi) and the absorber placed in 54.7° to the incident beam to avoid texture effects. Spectral acquisition was obtained over 1024 channels in the velocity range −4.5 to +4.5 mm/s. Data acquired on an α-Fe foil before folding were used for data calibration. The spectrum was fitted using the software MossA (Prescher et al., 2012), with one quadrupole doublet assigned to Fe (III) and two doublets assigned to Fe (II), applying Lorentzian line shapes and equal intensities of the quadrupole components.

### 2.4. Durability in simulated body fluids

#### 2.4.1. Dissolution test

Dissolution experiments were conducted under static conditions, using a modified Gamble solution (MGS: NaCl 112.3 mM and $Na_2SO_4{\cdot}10H_2O$ 0.556 mM), with the addition of 0.150 mM Na-citrate ($Na_3C_6H_5O_7{*}2H_2O$) as a chelating agent (Rozalen et al., 2013). Ultrapure deionized water (18.2 MΩ cm at 25 °C) was obtained from a MilliQ Element system (Millipore). All reagents were from Carlo Erba Reagents (DASIT Group, Milan, Italy). The solution pH was adjusted to the starting value of 4.5 with the addition of HCl. It must be pointed out that, even if the adopted conditions are far from mimicking the complexity of a cellular system, they may predict the dissolution dynamics occurring in vivo, in a reasonable experimental time, when the fibres are exposed to the lysosomal fluid during alveolar macrophage phagocytosis.

Powder samples (20 mg) were suspended in MGS (40 mL), placed in a polypropylene Falcon™ tube (BD Falcon™, Corning, Mexico) and continuously shaken in a thermostatic oscillating bath at 37 ± 1 °C. Experiments were conducted in quadruplicate for 1 h, 24 h, and 168 h (1 week) and a blank procedure was always carried out. For each experiment the solution was sampled with a syringe from the tube and filtered using 0.22 μm GSWP nitrocellulose membrane filters (Millex-HA, Millipore, Ireland). The concentration of the leached cations from the fibres in the supernatant was measured by Inductively coupled plasma optical emission spectroscopy (ICP-OES). To prevent oxidation, samples were stored in a glovebox under argon prior to XPS analysis.

#### 2.4.2. Inductively coupled plasma optical emission spectroscopy (ICP-OES)

Each filtered solution, properly diluted with a 1 % nitric acid solution, was analysed by ICP-OES to measure the concentration of leached Si, Mg, and Fe from the antigorite fibres. The measurements were performed using a Perkin–Elmer Optima 2000 DV ICP-OES spectrometer (Perkin-Elmer, Norwalk, CT, USA) equipped with a cyclonic spray chamber. ICP Aristar (BDH) standard solutions in nitric acid for the investigated elements were used to prepare the calibrating solutions for ICP-OES analysis.

#### 2.4.3. X-ray photoelectron spectroscopy (XPS)

XPS investigation was performed to determine the quantitative surface composition of the antigorite fibres before and after the dissolution tests. Analyses were performed using a Theta Probe spectrometer (Thermo Fisher Scientific, East Grinstead, UK) equipped with a monochromatic source (Al $k\alpha_{1,2}$ energy = 1486.6 eV). Survey spectra were acquired in fixed analyser transmission (FAT) mode with a pass energy of 200 eV, while high-resolution spectra were collected using a pass energy of 100 eV. The residual pressure during the analysis was below $10^{-7}$ Pa. The emission angle was 53° with respect to the perpendicular to the sample surface, and the angle between the source and the analyser axis was 63.78°. The instrument is also equipped with a low-energy electron/$Ar^+$ ion flood gun for charge compensation. The binding energy values were referred to the adventitious aliphatic carbon at 285.0 eV. Pristine samples were analysed as powders deposited on indium foil. Samples incubated for one week in the MGS solution were analysed as powder deposited on nitrocellulose membrane filters.

The spectra were processed using CasaXPS software. Fantauzzi et al. (2010) provides further experimental details (spectrometer calibration, linearity of the binding energy check according to ISO 15472:2010, spectra acquisition conditions and spectra fitting).

### 2.5. Surface chemical reactivity

Hydroxyl (•OH) and carboxyl radicals ($^{\bullet}COO^-$) generated by antigorite fibres were measured by spin trapping technique associated with Electron Paramagnetic Resonance (EPR), using Miniscope 100 EPR spectrometer (Magnettech, Berlin, Germany). 5,5-dimethylpirroline-N-oxide (DMPO; Cayman Chemical Company) was used as a spin trap. All other reagents were from Merck (Germany). The following experimental conditions were adopted: microwave power, 10 mW; modulation, 1 G; scan range, 120 G; centre of field 3330 G, gain $9{\cdot}10^2$.

For the generation of hydroxyl radicals, 10 mg of sample were suspended in 200 μL of 0.5 M potassium phosphate buffer (pH 7.4) and 100 μL of DMPO (0.18 M). The reaction was initiated by adding 100 μL of $H_2O_2$ (0.2 M). The release of hydroxyl radicals in the presence of $H_2O_2$ serves as a probe for Fenton and Fenton-like reactivity. For the generation of carboxyl radicals, 10 mg of sample were suspended in 100 μL of DMPO (0.18 M) and 100 μL of ultrapure MilliQ water. The reaction was started by adding 200 μL of sodium formate (2 M) in 1 M phosphate buffer (pH 7.4). The experiments were repeated in a reducing environment by adding 100 μL of ascorbic acid (6 mM) instead of ultrapure water. Formate ion was used as a model target molecule for the homolytic cleavage of a carbon-hydrogen bond in organic molecules. All tests were performed at 37 °C, in the absence of light and the EPR spectra were recorded on 50 μL of suspension after 10, 30, and 60 min of incubation with the target molecules. The amount of radical released is proportional to the intensity of the EPR signal. Generation of free radicals was investigated both on pristine samples and on samples incubated for 1 and 7 days in MGS. The experiments were performed at least in duplicate and a method blank, made by operating under the same conditions except that no solid particulate is introduced into the solution, was always carried out.

## 3. Results and discussion

### 3.1. Field and petrographic description

The investigated site is located near the village of San Mango d'Aquino (Catanzaro province) in Calabria, Southern Italy. The NOA-bearing ophiolite bodies present in this area belong to the Gimigliano-Monte Reventino Unit, part of the oceanic Southern Ligurian Domain included in the tectonic nappe system of the Calabrian-Peloritan Arc (Fig. 1a). The Gimigliano-Monte Reventino Unit consists of serpentinites and metabasites (metabasalts and minor metagabbros) and the relevant metasedimentary cover represented by quartzites (meta-radiolarites), marbles and calc-schists (Ogniben, 1973; Amodio-Morelli et al., 1976; Vitale et al., 2019). This unit registered a blueschist-facies peak metamorphism, followed by a diffuse retrogression under greenschist-facies

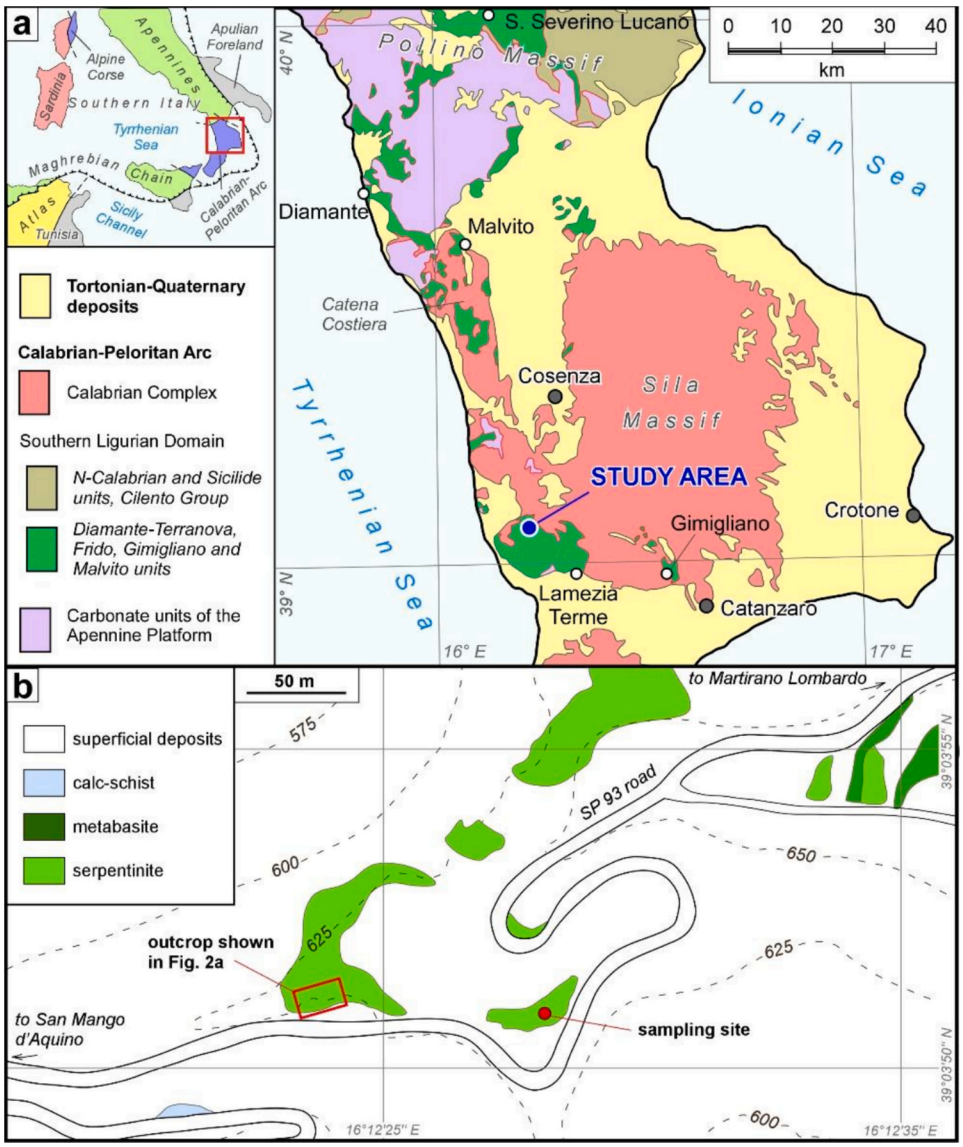



**Fig. 1.** a) Geological scheme of northern Calabria showing the distribution of the ophiolite-bearing units of the Southern Ligurian Domain and the position of the study area; modified after Amodio-Morelli et al. (1976). The inset shows the position of northern Calabria (red rectangle) in southern Italy. b) Scheme of the sampling area showing the position of the ophiolite outcrops and of the sampling site.

conditions associated with the development of the main foliation (Rossetti et al., 2002; Alvarez, 2005). Some portions of the meta-ophiolite bodies of the Gimigliano-Monte Reventino Unit were already characterized for their NOA content by Bloise et al. (2014), Punturo et al. (2015), and Campopiano et al. (2018a,b). These authors reported the occurrence of asbestos tremolite-actinolite, chrysotile and fibrous antigorite.

The sample was collected from an antigorite serpentinite body cropping out along the SP93 road at coordinates 39°03′50.9″N, 16°12′28.2″E (Fig. 1b). The outcrop consists of brecciated antigorite serpentinite, subdivided in dm- to m-large, lens-shaped lithons separated by mm- to cm-thick, anastomosing cataclastic zones (Fig. 2a), locally cemented by carbonate and fibrous tremolite. Serpentinite lithons are cut by abundant, mm- to cm-thick antigorite veins; the largest veins are located at the margins of the lithons, where they are commonly disrupted by later cataclastic processes that preferentially reactivated the already existing veins. The serpentinite bodies are also cut by sub-vertical faults with a N-S strike, coated by mm-thick, beige-coloured fibrous sepiolite layers associated with calcite commonly showing a slicken fibre growth.

The antigorite veins present either a cross-fibre or a slip fibre arrangement. At the mesoscale, they show a pale green colour with fairly pronounced silky lustre (Fig. 2b). They tend to split into mm-large and mm- to cm-long, lath-shaped elongated fragments (Fig. 2c). Under the optical microscope, the antigorite is colourless to very pale green and shows a fibrous growth habit (Fig. 2d, e); locally, growth zones parallel to the vein salvages, with a spacing of a few tens of micrometres, are present (Fig. 2e). The veins are locally deformed, as indicated by undulose extinction of antigorite fibres (Fig. 2d).

The sample used in this study was sampled from a portion of a cm-thick vein preserved at the margin of a serpentinite lithon, showing slip fibres, several centimetres long, with a marked fibrous appearance (Fig. 2b, c).

The San Mango d'Aquino site was selected after a geological survey which encompassed numerous serpentinite bodies belonging to the Gimigliano-Monte Reventino Unit in several localities of central Calabria. The serpentinite body cropping out in San Mango d'Aquino is representative in terms of lithological and structural characteristics, and, therefore, in terms of abundance, geometry and mineralogy of the fibrous mineral veins developed within it.

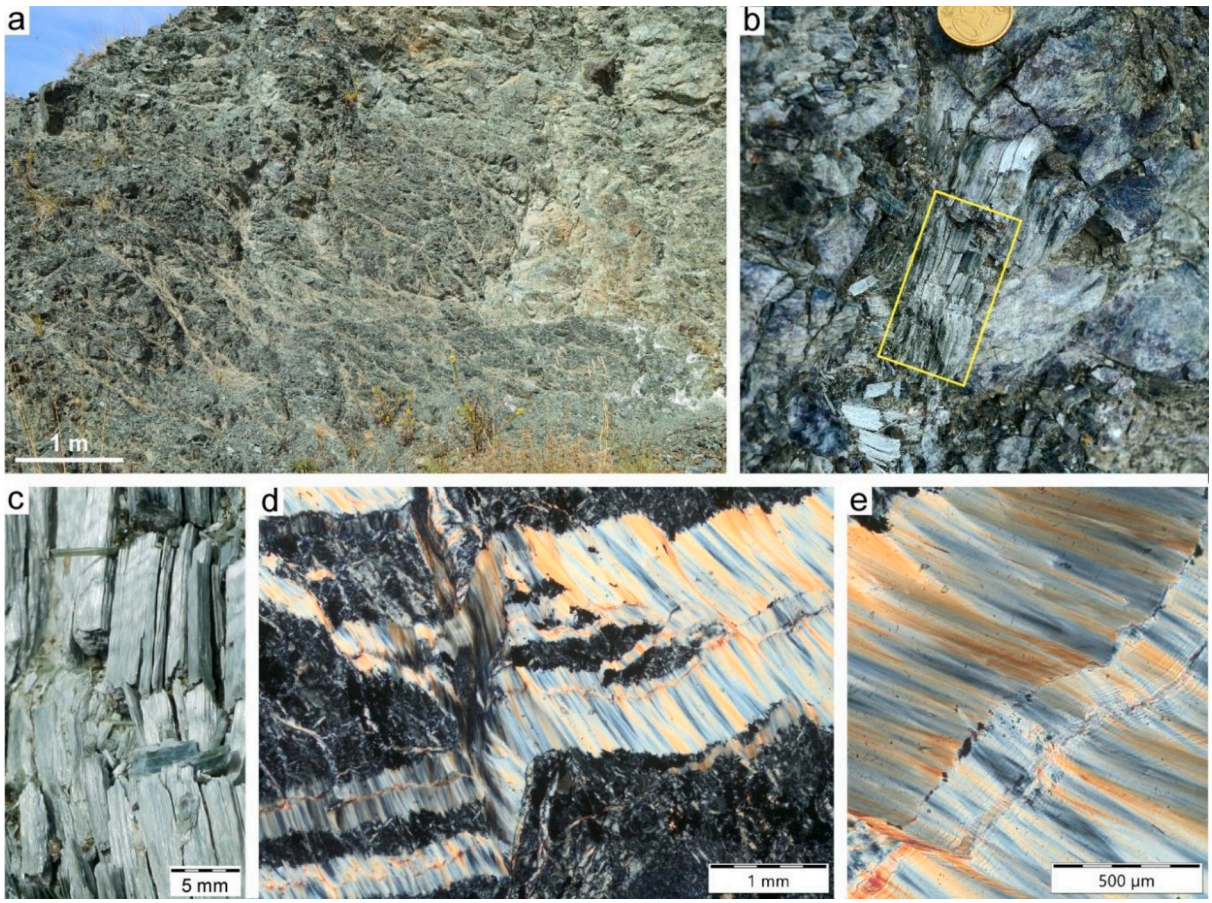



**Fig. 2.** a) Serpentinite antigorite outcrop of San Mango d'Aquino, showing lens-shaped, dm- to m- large lithons separated by anastomosing cataclastic bands. b) Portion of a cm-large antigorite vein preserved at the margin of an antigorite serpentinite lithon; from this vein portion was sampled the fibrous antigorite studied in this paper. c) Detail of the vein in b); note the mm-large, cm-long lath-shaped fragments derived from the splitting of the vein exposed to weathering agents. d, e) Thin section photomicrographs (cross-polarized light) of cross-fibre, mm-thick Atg veins cut parallel to the fibre elongation. Note the "fibrous" texture of antigorite, particularly evident in e).

More generally, the serpentinites of the Gimigliano-Monte Reventino Unit are comparable to those of the Palmaro-Caffarella Unit hosting the antigorite veins of the Varenna Valley site described by (Petriglieri et al., 2023). Both units are in fact composed of metaophiolites belonging to the Mesozoic Ligurian oceanic domain and underwent a similar metamorphic history with blueschist-facies peak conditions and a diffused greenschist-facies overprint. This similarity is mirrored by the characteristics of the fibrous mineral veins that developed in the serpentinites of both units, showing strict analogies in terms of geometric features (abundance, length, thickness) and mineralogical composition.

### 3.2. Morphological investigation

To validate whether antigorite from San Mango displays an asbestos-like morphology, we adopted the standardized mechanical stress, designed in Petriglieri et al. (2023). Antigorite sample was comminuted at four time points (2, 5, 10, and 20 min for comminution, see Par. 2.2.i). Morphometric parameters, encompassing particles and fibre size distribution, were carried out for each milling time and then compared with data obtained on fibrous asbestos-like antigorite and UICC crocidolite standard, selected as positive control samples displaying the asbestos-like morphology (Petriglieri et al., 2023).

The stacked bar chart (Fig. 3) reports the occurrence of % of particles (aspect ratio, AR $<$ 3), and EMPs (AR $>$ 3, following NIOSH, 2011 definition). EMPs are reported as respirable WHO (World Health Organization) fibres (AR $>$ 3, Length L $>$ 5 μm, Width W $<$ 3 μm, following definition by WHO, 1997), and non-respirable fibres (AR $>$ 3, W $>$ 3 μm).

As shown in Fig. 3, antigorite from San Mango preserved its fibrous nature with increasing comminution times. The percentage of EMPs (AR $>$ 3) and respirable WHO fibres (AR $>$ 3, L $>$ 5 μm, W $<$ 3 μm) did not significantly decrease, varying from 76 % to 66 % and from 35 % to 31 %, from 2 min to 20 min of comminution time, respectively. During milling, most antigorite elongated particles separated longitudinally, along the elongation growth axis, into thinner EMPs and respirable WHO fibres. A small amount of non-respirable fibres reduced its average length, splitting perpendicular to the growth axis, and resulting in a higher content of isometric particles, i.e. the % particles increased from 24 % to 34 % from 2 min to 20 min of comminution time.

Comminution of antigorite from Val Varenna (VV, Fig. 3) generated % of EMPs in the range 67–68 %, the 30 % of which of respirable WHO fibres. UICC crocidolite % of EMPs was 83 %, 47 % of which of WHO respirable fibres. Indeed, the high percentage of EMPs and WHO fibres measured for antigorite from San Mango placed in the range of fibrosity of asbestos and asbestos-like minerals. Comminuted EMPs and respirable fibres (WHO fibres) from San Mango antigorite preferentially showed a reduction of the width of elongated crystals with respect to their length (detailed morphological characterization of the Atg sample that is investigated in this paper is reported in Fig. S1), meeting the dimensional criteria that are relevant to define a hazardous mineral fibres (WHO, 1997). Representative SEM images of comminuted antigorite at 2 min and 20 min displayed the typical asbestos-like morphology of asbestos respirable fibres (Fig. 4). The adoption of the standardized milling procedure designed in previous work (Petriglieri

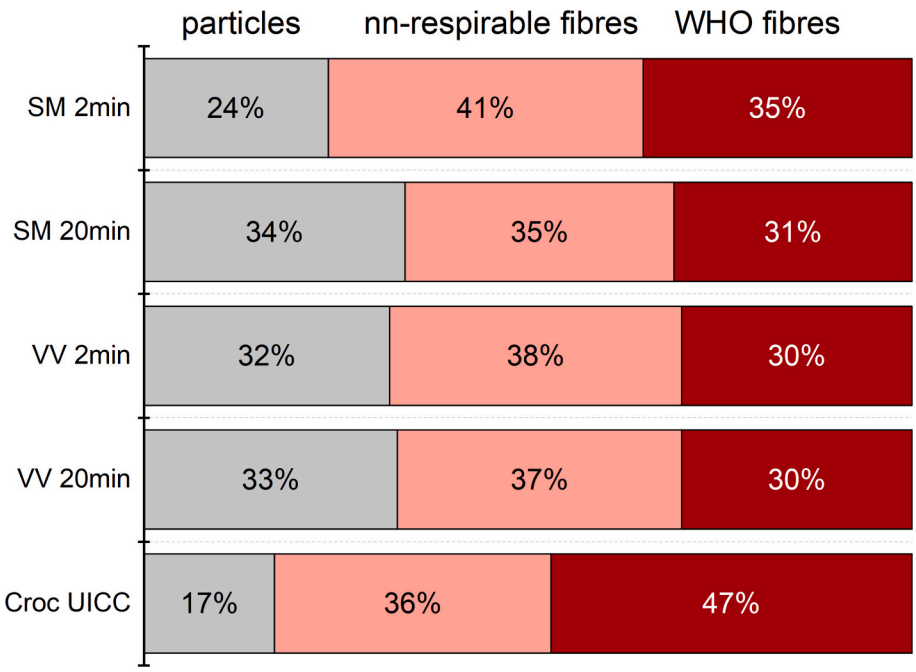



**Fig. 3.** Particle and fibre distribution of antigorite from San Mango (SM) after standardized mechanical milling (2 and 20 min) detected by optical microscopy and automated image analysis (FPIA). Stacked bar plot shows the % of objects with AR < 3 (particles, grey); AR > 3 (EMPs, according to NIOSH definition [NIOSH, 2011], light red) and respirable WHO fibres (AR > 3, W < 3 μm, L > 5 μm; [WHO, 1997], red). Varenna Valley antigorite (VV; Petriglieri et al., 2023) and UICC crocidolite (Croc UICC) were added for comparison. Full details of particle size distribution of antigorite from San Mango are reported in Supplementary materials S1.

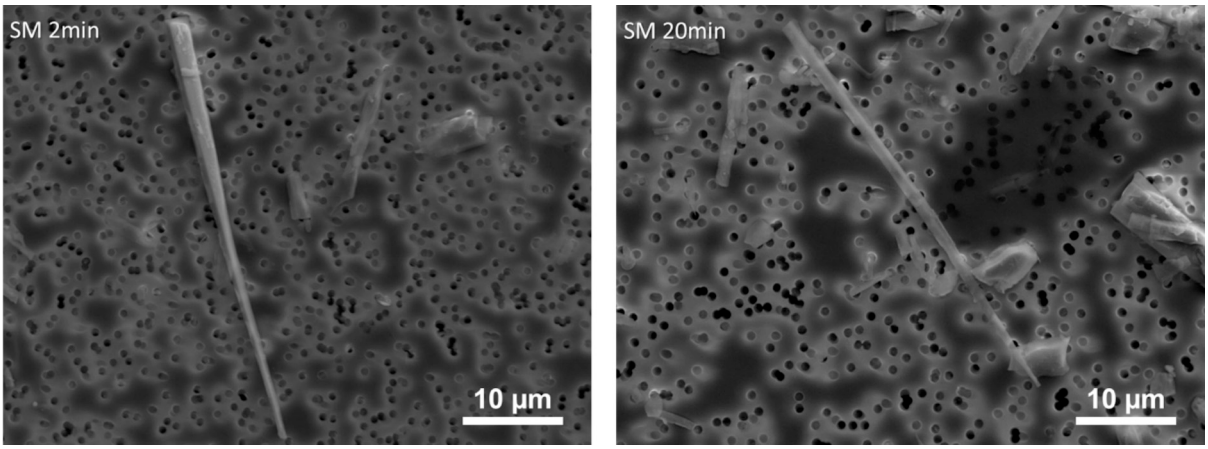



**Fig. 4.** Representative SEM images of respirable WHO antigorite fibres from San Mango after milling for 2 min and 20 min, showing the asbestos-like morphology.

et al., 2023) confirmed to be a discriminative approach to recognize the asbestos-like morphology of antigorite mineralizations that show fibrous to lamellar morphology at the macroscopic scale.

Further validation of this mechanical test is being performed on a complete set of macroscopically fibrous to lamellar NOA and EMPs, whose potential hazard is currently under debate.

### 3.3. Mineralogical investigation of antigorite fibres

The mineralogical investigation of antigorite fibres was performed by using a well-tested multi-analytical approach including Powder X-Ray Diffraction (PXRD), Transmission Electron Microscopy (TEM), Mössbauer spectroscopy, and Electron Microprobe Analysis (EMPA).

The average superstructure of antigorite from San Mango was determined following the approach of Uehara (1998) that is based upon the identification and measurement of the position of the first to third-order satellite reflections of $h_s$,0,1 type (where $h_s = 0 \pm u/M$, u = 1,2,3, and M = number of subcells) (Fig. 5b). Uehara and Shirozu (1985) demonstrated that the difference between the position of the 001 and ±3/M,0,1 reflections (indicated as Δ2θ) is modulated by the supercell M value (number of sub-cells having an *a* parameter of ca. 5.44 Å) because both *c* parameter and ß angle are relatively constant in antigorite samples. The diffraction pattern (Fig. 5) shows significantly broad superstructure reflections, in agreement with the coexistence of different antigorite polysomes observed by TEM (see below). The Δ2θ value of 1.20°2θ (Fig. 5b) corresponds to the M value of 8.508, as calculated from the regression eq. $M = 11.42 - 2.41 \times \Delta 2\theta$ proposed by Uehara (1998). From the relationship M = (m− 1) / 2 it is possible to derive the number of tetrahedra (m) occurring into the superstructure, i.e. the type of antigorite polysome that in the case of antigorite from San Mango is prevalently the m = 18 polysome (Capitani and Mellini, 2004). This polysome crystallises in a *C* centred space group (*C*2/*m*). In total each supercell contains 18 tetrahedra and 17 octahedra.

Diffraction patterns of the pristine and 1 week suspended in MGS

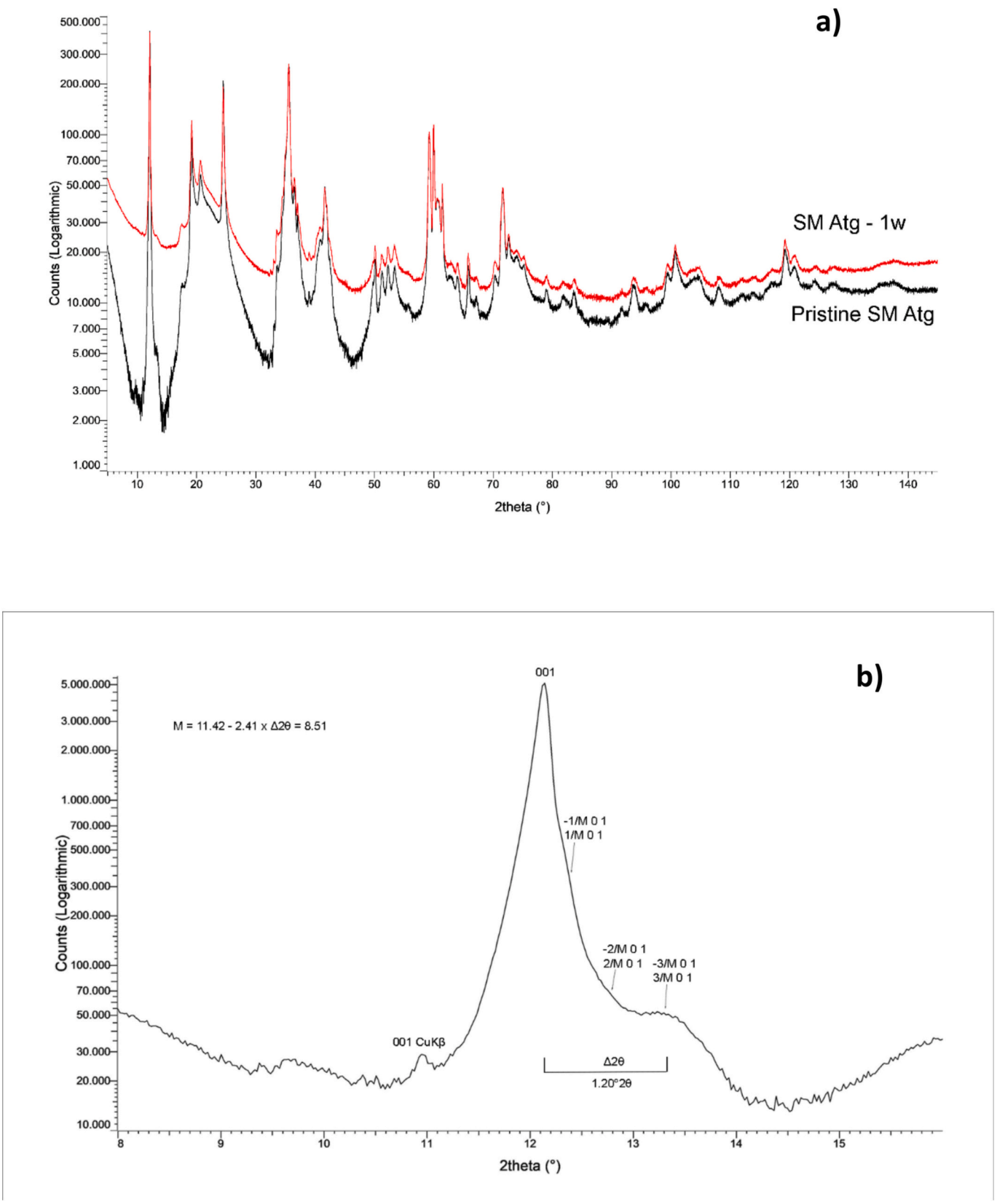



**Fig. 5.** a) Comparison of the diffraction patterns of pristine antigorite from San Mango (SM Atg) and sample after 1 week of incubation in MGS (SM Atg – 1w); b) magnified view of the diffraction pattern of antigorite from San Mango (intensity shown in logarithmic scale). Position of the first to third-order superstructure reflections is indicated.

samples are indistinguishable (Fig. 5a), suggesting no significant fibre alteration following dissolution process.

TEM investigation of the fibrous antigorite from San Mango revealed that antigorite structure is moderately disordered in terms of polysomatic disorder (varying wavelength of the TO-layer) but highly disordered in terms of polytypic disorder (different stacking of the TO-layer; Capitani and Mellini, 2005, 2007). The degree of disorder was assessed examining both selected area electron diffraction (SAED) patterns (Fig. 6) and HRTEM images (Fig. S2 in Supporting material). Several diffracting rows (from 4 to 6) in several SAED patterns taken along the [001] direction (Fig. 6c) were measured along the [100]* direction. The resulting *a* parameter varies from ~45.0 to ~54.0 Å, with an average value of 49.8 Å, corresponding to m = 20 polysomes (18 ≤ m ≤ 21). On HRTEM images, the *a* parameter was evaluated by measuring one-two packages of (100) lattice fringes in several images (19). The resulting average *a* value is ~50.2 Å, also in this case corresponding to the m = 20 polysome, consistently with the SAED results, even if locally the m value may have larger fluctuations (from 41.2 to 65.1 Å; 16 ≤ m ≤ 26). In comparison with polysomatic disorder, judging from the only one crystal found in the suitable [100] orientation, polytypic disorder, which arises from ±*b*/3 shift of the TO-layer, seems much more pronounced (compare streaking in Fig. 6b and d). Finally, from [001] SAED patterns, it appears that the direction of the superstructure modulation is not aligned with the a vector of the antigorite subcell (Fig. 6d), suggesting a triclinic symmetry instead of the documented monoclinic one (Capitani and Mellini, 2004, 2006). Keeping in mind the different volume analysed by HRTEM and PXRD, results are fully consistent.

The experimental Mössbauer spectrum of fibrous antigorite from San Mango (Fig. 7) was reproduced by the convolution of three doublets representing Fe (II) and Fe (III) ionic species. The spectrum was fitted following previous fitting models (Rozenson et al., 1979; Mellini et al., 2002), resulting in hyperfine parameters in very good agreement with those reported for fibrous antigorite from Val Varenna (Petriglieri et al., 2023). In particular, the two doublets with a large quadrupole splitting (QS) are typical for Fe (II), and the superimposed doublet with a smaller quadrupole splitting is typical for Fe (III). Notably, the minor difference isomer shift (IS) and a larger difference in quadrupole splitting observed for the two Fe (II) doublets (Fig. 7) may be attributed to next-nearest neighbour effects involving Mg, Fe (II) and Fe (III). Moreover, the broad envelope of the $Fe^{3+}$ doublet indicates possible presence of Fe (III) in both tetrahedral and octahedral sites, although limited spectral resolution did not allow to resolve the doublets by curve fitting. The Fe (III)/$Fe_{tot}$ ratio obtained from area measurement was 0.18, which indicates that this sample is less oxidized than antigorite from Val Varenna [Fe (III)/$Fe_{tot}$ ratio of 0.31].

EMPA analyses suggest chemical homogeneity of the fibres, being differences for major elements below 4 % relative (Table 1). The formula was normalized based on 8.668 oxygen atoms. This value derives from the general empirical formula of antigorite reported by Kunze (1961):

$$^{VI}M_{3m-3}{}^{IV}T_{2m}O_{5m}(OH)_{4m-6}$$

with M = Mg, Fe, Ni, Al; T = Si, Al; m = number of unique tetrahedra along the modulation wavelength, calculated assuming a representative m = 18, based on XRPD results. In the absence of clear indication, all Fe

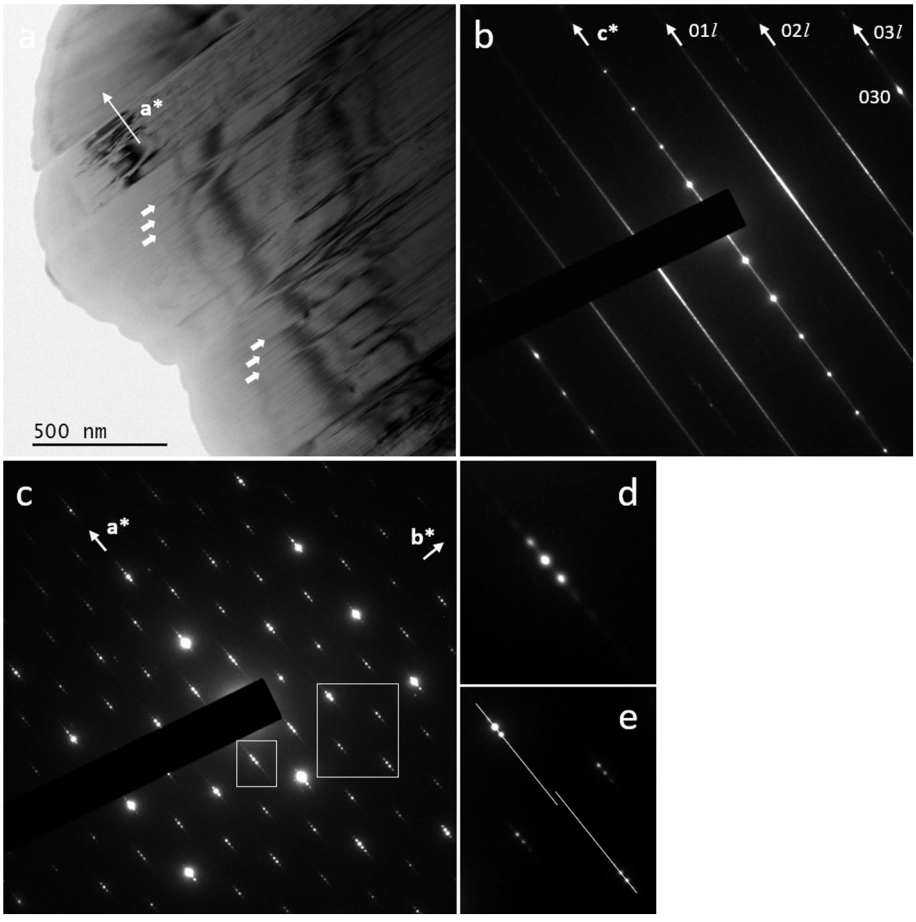
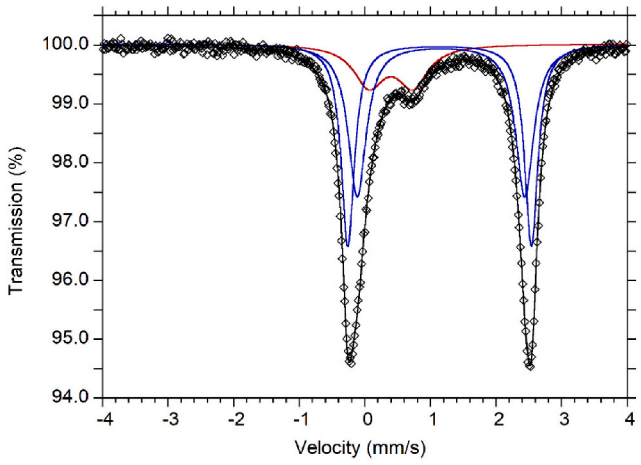



**Fig. 6.** (a) Bright-field image of fibrous antigorite from San Mango showing abundant stacking faults (arrows) perpendicular to a*. (b) SAED pattern taken along [100]. Note that 0*kl* rows show strong diffuse streaking along c* suggesting abundant polytypic disorder. (c) SAED patterns taken along [001]. (d) Magnified view of the smaller white box in (b). Note the weak diffuse streaking along a*, suggesting polysomatic disorder. (e) Magnified view of the larger white box in (c). Note how the direction of the superstructure modulation is not aligned with the subcell a* vector, suggesting a triclinic structure.




| IS (mm/s) | QS (mm/s) | FWHM (mm/s) | Assignment | Area (%) |
|---|---|---|---|---|
| 1.137(2) | 2.80(1) | 0.24(1) | Fe (II) | 40(4) |
| 1.159(3) | 2.55(2) | 0.33(1) | Fe (II) | 42(4) |
| 0.40(1) | 0.67(2) | 0.56(4) | Fe (III) | 18(2) |

**Fig. 7.** Room temperature $^{57}$Fe Mössbauer spectrum and parameters of fibrous antigorite from San Mango. Fitted absorption doublets assigned to Fe (II) are indicated in blue and Fe (III) in red. Diamonds denote the measured spectrum, and black curve represents the summed fitted spectrum. The table below the figure shows the $^{57}$Fe Mössbauer parameters for the three doublets: Isomer shift (IS) quadrupole splitting (QS), peak FWHM, and peak area (%).

**Table 1**
Chemical composition and empirical formulas (as atoms per formula unit, apfu) of fibrous antigorite from San Mango. Estimated standard deviation in brackets. Data of fibrous antigorite of Val Varenna (Petriglieri et al., 2023) are reported for comparison.

| | Antigorite San Mango | Antigorite Val Varenna | | Antigorite San Mango | Antigorite Val Varenna |
|---|---|---|---|---|---|
| Oxides | wt% | wt% | Sites | apfu | apfu |
| $SiO_2$ | 43.23(42) | 42.47(45) | Si | 1.984 | 1.973 |
| $Al_2O_3$ | 0.79(7) | 1.36(7) | $^{IV}$Al | 0.016 | 0.027 |
| MgO | 38.94(51) | 37.87(48) | ∑T | 2 | 2 |
| MnO | 0.10(3) | 0.15(3) | | | |
| $FeO_{tot}$ | 3.21(12) | 3.08(7) | $^{VI}$Al | 0.027 | 0.047 |
| $H_2O$[a] | 11.97 | 11.76 | Mg | 2.664 | 2.622 |
| Total | 98.32 | 96.67 | Mn | 0.004 | 0.006 |
| | | | Fe (II) | 0.101 | 0.083 |
| | | | Fe (III) | 0.023 | 0.037 |
| FeO[b] | 2.62 | 2.12 | ∑M | 2.818 | 2.795 |
| $Fe_2O_3$[b] | 0.66 | 1.06 | | | |
| | | | O | 5 | 5 |
| | | | OH | 3.668 | 3.647 |

[a] Calculated from stoichiometry.
[b] Measured by Mössbauer spectroscopy.

(III) was allocated at the octahedral sites. Due to the sum (Si + Al) in tetrahedral sites > 2 apfu, excess of Al was allocated in the octahedral layer. Comparison with chemical data obtained on fibrous antigorite from Val Varenna evidenced that the two samples significantly differ only in the total Al content (Table 1).

### 3.4. Durability and surface modifications of antigorite fibres in modified Gamble's solution (MGS)

The durability of antigorite fibres in MGS at pH 4.5 up to 1 week (168 h) was evaluated by measuring the released cations from the fibres by inductively coupled plasma - optical emission spectroscopy (ICP - OES). Results were compared with those obtained by Petriglieri et al. (2023) on UICC chrysotile and fibrous antigorite from Val Varenna, investigated under the same experimental conditions. Possible fibre surface chemical modifications following incubation in MGS were studied by X-ray photoelectron spectroscopy (XPS).

Results of ICP-OES analyses are reported in Fig. 8. Both Si and Mg release progressively increased with time, ranging from 207(8) mg/kg and 734(35) mg/kg after 1 h up to 2765(83) mg/kg and 3170(109) mg/kg after 1 week (168 h), respectively. Moreover, minor Fe and Al release occurred (Supplementary materials, Table S1). Regarding Fe, the observed decrease in concentration within the solution after the first 24 h of fibre incubation suggests possible precipitation of secondary phases as Fe-oxyhydroxides. Besides, XRPD analysis did not reveal any occurrence of mineral precipitates in the leached samples, indicating that the neo-formed phases are likely amorphous. It should be pointed out that the cation release is likely enhanced by the presence of citrate ($Na_3C_6H_5O_7$) in the leaching solution, acting as a chelating (Glusker, 1980).

The comparison between antigorite from San Mango with that from Val Varenna highlighted that the dissolution kinetics of the two samples are almost the same (Fig. 8). Besides, the progression of the cation dissolution further revealed the existence of two regions: (1) between zero and 24 h, representing the conditions of undersaturation, favourable to fibre dissolution; (2) after 24 h, representing the near-saturation conditions, where cation release rate is much lower (Petriglieri et al., 2023).

UICC chrysotile shows a markedly higher cation release for the entire duration of the experiment (Fig. 8). However, in the region of near-saturation conditions (after 24 h) a decrease in both Si and Mg release was observed, suggesting possible incorporation of these elements into neo-formed precipitates (Petriglieri et al., 2023).

To compare the durability of fibrous antigorite of this work with that of the Val Varenna sample and UICC chrysotile, dissolution rates were retrieved using Si release in the unsaturated region (0–24 h) normalized on BET sample surface area, being Si release the rate determining step for silicate dissolution (Oze and Solt, 2010). Results highlight that the Calabrian sample dissolves three times faster than the Ligurian one (dSi/dt = 10.5 nmol × $h^{-1}$ × $m^{-2}$ and dSi/dt = 3.6 nmol × $h^{-1}$ × $m^{-2}$, respectively). The faster rate observed for the San Mango antigorite is possibly related to its lower content of Al ions replacing Mg in the octahedral sheet [$(Al^{3+}/(Mg^{2+} + Al^{3+}))$ is 0.010 and 0.017 for San Mango and Val Varenna antigorite, respectively]. Madelung energies for Al—O and Mg—O in octahedral coordination are 0.50 and 0.33, respectively, and accordingly, Mg easily dissolve from the silicate structure. Surprisingly, San Mango antigorite showed a dissolution rate normalized on BET sample surface area even higher than that of UICC chrysotile (dSi/dt = 4.7 nmol × $h^{-1}$ × $m^{-2}$). However, cation leaching for chrysotile is certainly hindered due to the achievement for this sample of the saturation conditions in the early stages of dissolution process (within the first 24 h), and therefore cannot be easily compared with that of the two antigorite samples. Nevertheless, due to the low surface area of fibrous antigorite its resident time in vivo is expected to be higher than chrysotile. Besides, cation release was incongruent for chrysotile for the whole incubation time, while both antigorite samples reach a congruent Si and Mg release after the early steps of the dissolution process (Fig. 8). The preferential Mg release with respect to Si in first dissolution stages agrees with their differences in Madelung site energies (Petriglieri et al., 2023) and previous results of Gualtieri et al. (2018) showing that chrysotile rapidly undergoes amorphization in acidic medium with the formation of a silica-rich fibrous metastable pseudomorph.

Pristine and incubated fibrous antigorite samples were investigated by XPS to highlight any possible chemical modification following dissolution in MGS. Particular attention was paid to Fe due its primary role in fibre chemical reactivity and toxicity (Fubini and Otero Aréan, 1999; Kamp and Weitzman, 1999). Table 2 shows the obtained results.

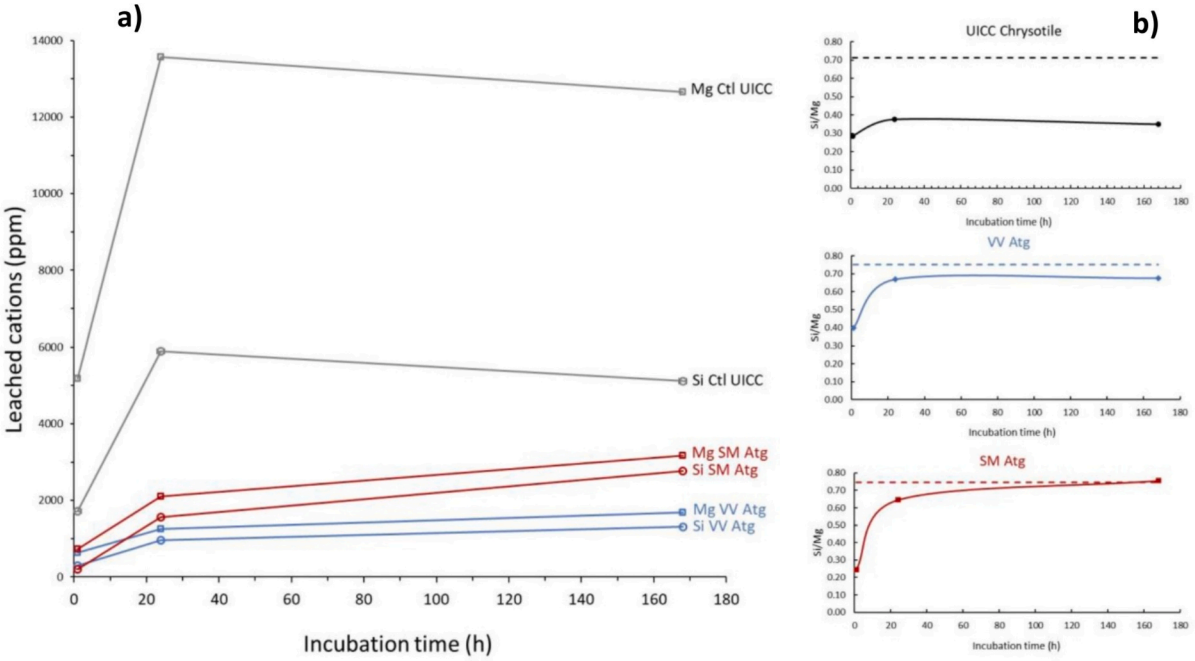



**Fig. 8.** a) Si and Mg release as a function of the incubation time of fibrous antigorite from San Mango (SM Atg). Results on antigorite from Val Varenna (VV Atg) and UICC chrysotile (Ctl UICC) are reported for comparison. Values are reported as means ± SD; b) variation of Si/Mg ratio in solution as a function of sample incubation time. Bulk Si/Mg ratio (dotted line) obtained from chemical analyses (by EMP) of the pristine sample is reported for comparison.

**Table 2**
XPS surface composition (at.%) and Fe speciation of antigorite from San Mango (SM Atg) before (pristine sample) and after dissolution in MGS at pH = 4.5 for 1 week (1 W). Mean values on three different areas of each sample are listed together with standard deviations (in parentheses). In addition, data of antigorite from Val Varenna (VV Atg) and UICC chrysotile (UICC Ctl) (Petriglieri et al., 2023) are reported for comparison (Fe speciation for chrysotile samples is not reported due to the low signal-to-noise ratio of Fe $2p_{3/2}$ peak). For San Mango antigorite, the bulk compositions in atomic percent, obtained by electron microprobe analysis, is reported.

| Samples | Composition (at.%) | | | | Fe speciation (%) | | |
|---|---|---|---|---|---|---|---|
| | O | Si | Mg | Fe | Fe (II)-O | Fe (III)-O | Fe (III)-OOH |
| SM Atg – Bulk[a] | 64 | 15 | 20 | 1 | 82(8) | 18(2) | – |
| SM Atg – Pristine | 64(2) | 16 (1) | 19 (1) | 1.4 (0.2) | 49(2) | 10(2) | 41(2) |
| SM Atg – 1 W | 57(1) | 20 (1) | 21 (1) | 1.7 (0.3) | 53(2) | 6(1) | 41(3) |
| VV Atg – Pristine | 60(2) | 19 (1) | 20 (1) | 1.0 (0.2) | 41(2) | 20(1) | 39(3) |
| VV Atg – 1 W | 58(1) | 19 (1) | 22 (2) | 1.0 (0.3) | 40(5) | 10(2) | 50(3) |
| UICC Ctl – Pristine | 61.8 (0.1) | 14 (1) | 24 (1) | 0.2 (0.1) | | | |
| UICC Ctl – 1 W | 63.0 (0.2) | 13 (1) | 23 (1) | 1.0 (0.2) | | | |

[a] Uncertainty ± 1 % for O, Si, Mg, and ±5 % for Fe. N.d.

Survey spectra and peak binding energy values of pristine and incubated samples up to one week in MGS are reported in Supporting material (Fig. S3 and Table S2, respectively). The surface Fe speciation was obtained by fitting the high-resolution Fe $2p_{3/2}$ signal (Fig. S2), following the approach of Fantauzzi et al. (2010). No signals from sodium, sulphur and chlorine were detected, indicating that no residues from the incubating solutions are present on the mineral surface.

The surface composition of the pristine fibres was comparable to that of the bulk, except for a difference in Fe oxidation state. In particular, the iron at the fibre surface is much more oxidized than the bulk, and a the significant amount of the Fe (III) (ca. 40 %) is present as FeOOH oxihydroxide (Table 2), possibly due to weathering processes (Schott and Berner, 1983). It must be noted that, for both the Calabrian and Ligurian antigorite samples, the fibre surface after incubation up to 1 week in MGS showed no significant differences in the cation content compared to that of the pristine ones, in agreement with the congruent behaviour of the dissolution process. Conversely, the incongruent dissolution of chrysotile is well documented by the Fe enrichment observed for the incubated sample (Table 2), in line with ICP-OES results showing that Fe leaching rate is negligible compared to both Si and Mg release (Petriglieri et al., 2023).

Concerning surface Fe speciation, fibrous antigorite from San Mango did not show significant differences following dissolution in MGS. Differently, fibrous antigorite from Val Varenna shows a significant increase of the FeOOH component at the expense of the Fe (III)-O component, after 1 week of incubation in MGS (Table 2). This result is in line with the lower solubility of the Ligurian sample, hindering the exposure on the fibre surface of new Fe sites from the bulk and leading to the conversion of surface Fe into FeOOH (Petriglieri et al., 2023), supposed to be in the outer part of the mineral surface (Fantauzzi et al., 2010; Pacella et al., 2021). In the case of chrysotile sample, it was not possible to resolve the peak in its Fe (II) and Fe (III) components, due to the small amount of iron and the consequent low signal-to-noise ratio of the Fe $2p_{3/2}$ peak.

### 3.5. Surface chemical reactivity of antigorite fibres

Fibrous antigorite from San Mango was active in both hydroxyl and carboxyl radical generation (Fig. 9), although the latter was observed only in presence of ascorbic acid. This behaviour is commonly observed in natural fibres undergoing oxidative chemical weathering (Andreozzi et al., 2017; Gazzano et al., 2023), where the surface iron mainly occurs in the oxidized form. Ascorbic acid, indeed, promotes reduction of Fe (III) to Fe (II), which, when poorly coordinated, may catalyse homolytic cleavage of C—H bonds leading to carbon-centred radicals. Notably, for both Calabrian and Ligurian fibrous antigorite, the •OH production after

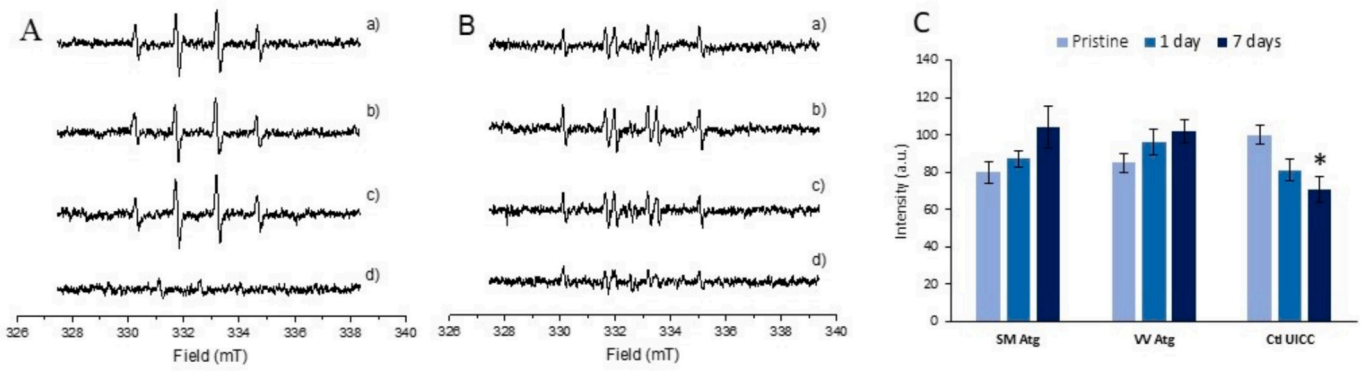



**Fig. 9.** Representative EPR spectra of (A) [DMPO-OH]• and (B) [DMPO-$COO^-$]• adducts recorded for (a) SM Atg, (b) VV Atg, (c) UICC chrysotile, and (d) blank after 1 h of incubation with the target molecule ($H_2O_2$ for •OH and $HCOO^-$ for carboxyl radical detection). The [DMPO-OH]• adduct signal is characterized by four peaks with intensity 1:2:2:1 and the [DMPO-$COO^-$]• signal by six peaks of equal intensity. The EPR signal of the ascorbyl radical, as intermediate in the oxidation of ascorbic acid to dehydroascorbic acid, was detected (signal at ca. 333 mT in panel B). (C) Amount of •OH radicals generated by the pristine and MGS-incubated (after 1 and 7 days) samples, obtained by double integration of the EPR spectra. Asterisk indicates significant difference between pristine and incubated fibres: $*p < 0.05$ (one-way ANOVA followed by post-hoc Tukey's test). Data for VV Atg and UICC chrysotile fibres from Petriglieri et al. (2023) are reported for comparison.

sample incubation in MGS up to 7 days is still comparable with that observed for the pristine ones.

Conversely, the progressive reduction of the Fenton-like reactivity observed for the MGS-incubated chrysotile samples was related to possible formation of secondary phases on the fibre surface (as suggested by ICP-OES data) that may mask the Fenton active Fe centres (Petriglieri et al., 2023). It must be pointed out that, the decreased reactivity of the leached chrysotile with respect to the pristine sample, does not correlate with its higher surface Fe content (Table 2), further supporting the hypothesis that the surface reactivity is dependent on specific low-coordinated surface Fe ions rather than the total Fe content of the mineral (Lim et al., 2006; Turci et al., 2011; Andreozzi et al., 2017).

## 4. Conclusions

NOA sites may represent a source of risk for the nearby resident population and attract the interest and concern of the environmental protection agencies. An appropriate approach is therefore required throughout the stages of site investigation for adequate risk assessment and management. Following a recently proposed innovative and interdisciplinary procedure designed to evaluate the hazard of NOA site hosting fibrous antigorite (Petriglieri et al., 2023), we have here investigated the key parameters that define the asbestos-like properties relevant to fibre toxicity from a NOA-rich antigorite serpentinite outcrop near San Mango D'Aquino, Calabrian Southern Apennines, Italy. The outcrop was selected after a field and petrographic geological study as representative of the serpentinites cropping out over a large area in central Calabria. San Mango antigorite showed up to 66 % of EMPs upon standardized mechanical stress, with a significant fraction (about 31 %) of respirable fibres, according to the WHO counting criteria. San Mango antigorite fibres showed a lower cation release than chrysotile driven by its lower surface area. The observed surface reactivity was comparable to that of fibrous antigorite from other sites in Ligurian Alps (i.e., Val Varenna, Genoa) and UICC chrysotile. Notably, radical generation activity is preserved upon fibre leaching in simulated body fluid (modified Gamble's solution) that promoted iron mobilization. Antigorite from San Mango outcrop share with chrysotile and other fibrous antigorite samples the key minero-chemical properties that indicate a possible asbestos-like behaviour. Exposure to San Mango antigorite may represent a risk for people living in proximity of the San Mango NOA site and other sites where serpentinites with similar geological features occur. To evaluate the exposure level, an investigation aimed at assessing the environmental exposure to airborne antigorite fibres in the area is currently ongoing. It is worth highlighting that the San Mango d'Aquino antigorite and the Val Varenna antigorite described by Petriglieri et al. (2023) derive from outcrops selected to be geologically representative of serpentinites cropping out over large areas in central Calabria and in the Genoa area, respectively. For this reason, we suggest that the presence of antigorite with asbestos-like behaviour in the two sites should not be regarded as an isolated occurrence, but as a potential feature of the antigorite serpentinite bodies of the two geological domains and of other geological domains with a comparable geological evolution.

## CRediT authorship contribution statement

**J.R. Petriglieri:** Writing – review & editing, Writing – original draft, Visualization, Methodology, Investigation. **G. Capitani:** Writing – review & editing, Writing – original draft, Visualization, Methodology, Investigation, Formal analysis. **P. Ballirano:** Writing – review & editing, Writing – original draft, Supervision, Methodology, Investigation. **L. Barale:** Writing – review & editing, Writing – original draft, Visualization, Validation, Resources, Methodology, Investigation. **F. Piana:** Writing – review & editing, Writing – original draft, Resources, Project administration, Methodology, Investigation. **M. Tomatis:** Visualization, Investigation, Formal analysis. **M.C. Di Carlo:** Investigation, Formal analysis. **F. Gianchiglia:** Investigation, Formal analysis. **A. Campopiano:** Supervision. **A. Olori:** Investigation. **M.R. Bruno:** Investigation. **M.R. Montereali:** Investigation, Formal analysis. **E. Nardi:** Investigation, Formal analysis. **M. Fantauzzi:** Writing – review & editing, Writing – original draft, Validation, Investigation, Formal analysis. **A. Rossi:** Writing – review & editing, Writing – original draft, Validation, Resources, Methodology. **H. Skogby:** Investigation, Formal analysis. **E. Belluso:** Supervision. **F. Turci:** Writing – review & editing, Writing – original draft, Supervision, Project administration, Methodology, Funding acquisition, Conceptualization. **A. Pacella:** Writing – review & editing, Writing – original draft, Supervision, Project administration, Methodology, Investigation, Funding acquisition, Formal analysis, Conceptualization.

## Declaration of competing interest

The authors declare that they have no known competing financial interests or personal relationships that could have appeared to influence the work reported in this paper.

## Acknowledgements

This project is funded by the INAIL - BRIC 2019 project (grant

number ID 57). Domenico Mannetta (Sapienza University of Rome) is thanked for the skilful realisation of the TEM sections. Marcello Serracino is kindly acknowledged for technical assistance for electron microprobe analysis (EMPA) at "Istituto di Geologia Ambientale e Geoingegneria" of the National Research Council (IGAG-CNR), Rome, Italy.

## Appendix A. Supplementary data

Supplementary data to this article can be found online at https://doi.org/10.1016/j.scitotenv.2025.178970.

## Data availability

Data will be made available on request.

## References

Alvarez, W., 2005. Structure of the Monte Reventino greenschist folds: a contribution to untangling the tectonic-transport history of Calabria, a key element in Italian tectonics. J. Struct. Geol. 27, 1355–1378.
Amodio-Morelli, L., Bonardi, G., Colonna, V., Dietrich, D., Giunta, G., Ippolito, F., Liguori, V., Lorenzoni, S., Paglionico, A., Perrone, V., Piccarreta, G., Russo, M., Scandone, P., Zanetti-Lorenzoni, E., Zuppetta, A., 1976. L'Arco Calabro-Peloritano nell'orogene appenninico-maghrebide. Mem. Soc. Geol. Ital. 17, 1–60.
Andreozzi, G.B., Pacella, A., Corazzari, I., Tomatis, M., Turci, F., 2017. Surface reactivity of amphibole asbestos: a comparison between crocidolite and tremolite. Sci. Rep. 7.
Anthony, J.W., Bideaux, R.A., Bladh, K.W., Nichols, M.C. (Eds.), 2001. Handbook of Mineralogy. Mineralogical Society of America, Chantilly, VA 20151-1110, USA.
Asgharian, B., Owen, T.P., Kuempel, E.D., Jarabek, A.M., 2018. Dosimetry of inhaled elongate mineral particles in the respiratory tract: the impact of shape factor. Toxicol. Appl. Pharmacol. 361, 27–35.
Baumann, F., 2012. Environmental exposure to carcinogenic fibers due to serpentinite paved roads in New Caledonia: lessons in environmental epidemiology and in prevention. In: Geological Society of America, Cordilleran Section, 108th Annual Meeting, Abstracts With Programs, 44, 3, 8.
Baumann, F., 2024. Environmental exposure to asbestos and cancer. In: Carbone, M., Dodson, R., Pass, H., Yang, H. (Eds.), Asbestos: Risk Assessment, Epidemiology, and Health Effects. CRC Press.
Baumann, F., Ambrosi, J., 2013. Environmental exposure to mineral fibers in New Caledonia: an ecological study. In: American Geophysical Union, Spring Meeting 2013, Abstract Id. B34A-02.
Baumann, F., Maurizot, P., Mangeas, M., Ambrosi, J.P., Douwes, J., Robineau, B., 2011. Pleural mesothelioma in New Caledonia: associations with environmental risk factors. Environ. Health Perspect. 119, 695–700.
Bayram, M., Bakan, N.D., 2014. Environmental exposure to asbestos: from geology to mesothelioma. Curr. Opin. Pulm. Med. 20, 301–307.
Berman, D.W., Crump, K.S., 2008. A meta-analysis of asbestos-related cancer risk that addresses fiber size and mineral type. Crit. Rev. Toxicol. 38 (Suppl. 1), 49–73.
Bloise, A., Critelli, T., Catalano, M., Apollaro, C., Miriello, D., Croce, A., Barrese, E., Liberi, F., Piluso, E., Rinaudo, C., Belluso, E., 2014. Asbestos and other fibrous minerals contained in the serpentinites of the Gimigliano-Mount Reventino Unit (Calabria, S-Italy). Environ. Earth Sci. 71, 3773–3786.
Bloise, A., Punturo, R., Catalano, M., Miriello, D., Cirrincione, R., 2016. Naturally occurring asbestos (NOA) in rock and soil and relation with human activities: the monitoring example of selected sites in Calabria (southern Italy). Ital. J. Geosci. 135 (2), 268–279.
Bloise, A., Catalano, M., Critelli, T., Apollaro, C., Miriello, D., 2017. Naturally occurring asbestos: potential for human exposure, San Severino Lucano (Basilicata, Southern Italy). Environ. Earth Sci. 76, 648.
Brunauer, S., Emmett, P.H., Teller, E., 1938. Adsorption of gases in multimolecular layers. J. Am. Chem. Soc. 60, 309–319.
Bruno, C., Tumino, R., Fazzo, L., Cascone, G., Cernigliaro, A., De Santis, M., Giurdanella, M.C., Nicita, C., Rollo, P.C., Scondotto, S., Spata, E., Zona, A., Comba, P., 2014. Incidence of pleural mesothelioma in a community exposed to fibres with fluoro-edenitic composition in Biancavilla (Sicily, Italy). Ann. Ist. Super. Sanità 50, 111–118.
Campopiano, A., Olori, A., Spadafora, A., Bruno, M.R., Angelosanto, F., Iannò, A., Casciardi, S., Giardino, R., Conte, M., Oranges, T., Iavicoli, S., 2018a. Asbestiform minerals in ophiolitic rocks of Calabria (southern Italy). Int. J. Environ. Health Res. 28 (2), 134–146.
Campopiano, A., Bruno, M.R., Olori, A., Angelosanto, F., Iannò, A., Casciardi, S., Spadafora, A., 2018b. Fibrous antigorite in Mount Reventino area of central Calabria. J. Mediter. Earth Sci. 10, 17–25.
Capitani, G.C., Mellini, M., 2004. The modulated crystal structure of antigorite: the m = 17 polysome. Am. Mineral. 89, 147–158.
Capitani, G., Mellini, M., 2005. HRTEM evidence for 8-reversals in the m = 17 antigorite polysome. Am. Mineral. 90, 991–999.
Capitani, G., Mellini, M., 2006. The crystal structure of a second antigorite polysome (m = 16), by single-crystal synchrotron diffraction. Am. Mineral. 91, 394–399.
Capitani, G., Mellini, M., 2007. High-resolution transmission electron microscopy (HRTEM) investigation of antigorite polysomes (m = 15 to 18). Am. Mineral. 92, 64–71.
Carbone, M., Emri, S., Dogan, A.U., Steele, I., Tuncer, M., Pass, H.I., Baris, Y.I., 2007. A mesothelioma epidemic in Cappadocia: scientific developments and unexpected social outcomes. Nat. Rev. Cancer 7, 147–154.
Cardile, V., Lombardo, L., Belluso, E., Panico, A., Capella, S., Balazy, M., 2007. Toxicity and carcinogenicity mechanisms of fibrous antigorite. Int. J. Environ. Res. 4, 1–9.
Cliff, G., Lorimer, G.W., 1975. The quantitative analysis of thin specimens. J. Microsc. 103, 203–207.
Cluzel, D., Boulvais, P., Iseppi, M., Lahondère, D., Lesimple, S., Maurizot, P., Paquette, J. L., Tarantola, A., Ulrich, M., 2020. Slab-derived origin of tremolite–antigorite veins in a supra-subduction ophiolite: the Peridotite Nappe (New Caledonia) as a case study. Int. J. Earth Sci. 109, 171–196.
Conconi, R., Ventruti, G., Nieto, F., Capitani, G., 2023. TEM-EDS microanalysis: comparison among the standardless, Cliff & Lorimer and absorption correction quantification methods. Ultramicroscopy 254, 113845.
Constantopoulos, S.H., 2008. Environmental mesothelioma associated with tremolite asbestos: lessons from the experiences of Turkey, Greece, Corsica, New Caledonia and Cyprus. Regul. Toxicol. Pharmacol. 52, 110–115.
Cox, L.A., Bogen, K.T., Conolly, R., Graham, U., Moolgavkar, S., Oberdorster, G., Roggli, V.L., Turci, F., Mossman, B., 2023. Mechanisms and shapes of causal exposure-response functions for asbestos in mesotheliomas and lung cancers. Environ. Res. 230, 115607.
Délibération n°82 du 25 août, 2010. Relative à la protection des travailleurs contre les poussières issues de terrains amiantifères dans les activités extractives, debâtiment et de travaux publics. JONC du 9 Septembre 2010.
Di Giuseppe, D., Perchiazzi, N., Brunelli, D., Giovanardi, T., Nodari, L., Della Ventura, G., Malferrari, D., Maia, M., Gualtieri, A.F., 2021. Occurrence and characterization of tremolite asbestos from the Mid Atlantic Ridge. Sci. Rep. 11, 6285.
Fantauzzi, M., Pacella, A., Atzei, D., Gianfagna, A., Andreozzi, G.B., Rossi, A., 2010. Combined use of X-ray photoelectron and Mössbauer spectroscopic techniques in the analytical characterization of iron oxidation state in amphibole asbestos. Anal. Bioanal. Chem. 396, 2889–2898.
Fitzgerald, S.M., Harty, E.A., 2014. Antigorite: is it the forgotten asbestos? Prof. Saf. 59 (8), 43–48.
Fubini, B., Otero Aréan, C., 1999. Chemical aspects of the toxicity of inhaled mineral dusts. Chem. Soc. Rev. 28, 373–381.
Gazzano, E., Petriglieri, J.R., Aldieri, E., Fubini, B., Pavan, C., Tomatis, M., Turci, F., 2023. Cytotoxicity of fibrous antigorite from New Caledonia. Environ. Res. 230, 115046.
Glusker, J.P., 1980. Citrate conformation and chelation: enzymatic implications. Acc. Chem. Res. 13, 45–352.
Groppo, C., Compagnoni, R., 2007. Ubiquitous fibrous antigorite veins from the Lanzo Ultramafic Massif, Internal Western Alps (Italy): characterization and genetic conditions. Period. Mineral. 76, 169–181.
Gualtieri, A.F., 2017. In: Gualtieri, A.F. (Ed.), Mineral Fibres: Crystal Chemistry, Chemical-Physical Properties, Biological Interaction and Toxicity. European Mineralogical Union and the Mineralogical Society of Great Britain & Ireland, p. 18.
Gualtieri, A.F., 2020. Naturally occurring asbestos: a global health concern? State of the art and open issues. Environ. Eng. Geosci. XXVI (1), 3–8.
Gualtieri, A.F., 2023. Journey to the centre of the lung. The perspective of a mineralogist on the carcinogenic effects of mineral fibres in the lungs. J. Hazard. Mater. 442.
Gualtieri, A.F., Pollastri, S., Gandolfi, N.B., Ronchetti, F., Albonico, C., Cavallo, A., Zanetti, G., Marini, P., Sala, O., 2014. Determination of the concentration of asbestos minerals in highly contaminated mine tailings: an example from abandoned mine waste of Cretaz and Emarese (Valle d'Aosta, Italy). Am. Mineral. 99 (7), 1233–1247.
Gualtieri, A.F., Pollastri, S., Gandolfi, N.B., Lassinantti Gualtieri, M., 2018. In vitro acellular dissolution of mineral fibres: a comparative study. Sci. Rep. 8 (1), 1–12.
Harper, M., 2008. 10th anniversary critical review: naturally occuring asbestos. J. Environ. Monit. 1373–1528.
Kamp, D.W., Weitzman, S.A., 1999. The molecular basis of asbestos induced lung injury. Thorax 54, 638–652.
Keeling, J., Raven, M.D., McClure, S.G., 2006. Identification of fibrous mineral from Rowland Flat area, Barossa Valley, South Australia. In: Department of Primary Industries and Resources. Report Book, 2006/2 (27 pp.).
Koumantakis, E., Kalliopi, A., Dimitrios, K., Gidarakos, E., 2009. Asbestos pollution in an inactive mine: determination of asbestos fibers in the deposit tailings and water. J. Hazard. Mater. 167, 1080–1088.
Kunze, G., 1961. Antigorite. Fortschr. Miner. 39, 206–324.
Lee, R.J., Strohmeier, B.R., Bunker, K.L., Van Orden, D.R., 2008. Naturally occurring asbestos—a recurring public policy challenge. J. Hazard. Mater. 153 (1–2), 1–21.
Lim, H., Lee, J., Jin, S., Kim, J., Yoon, J., Hyeon, T., 2006. Highly active heterogeneous Fenton catalyst using iron oxide nanoparticles immobilized in alumina coated mesoporous silica. Chem. Comm. 463–465.
Lippmann, M., 2009. Environmental Toxicants: Human Exposures and Their Health Effects, Third ed. John Wiley & Sons, Inc, Hoboken, NJ.
Luo, S., Liu, X., Mu, S., Tsai, S.P., Wen, C.P., 2003. Asbestos related diseases from environmental exposure to crocidolite in Da-yao, China. I. Review of exposure and epidemiological data. Occup. Environ. Med. 60, 35–41.
Mellini, M., Viti, C., 1994. Crystal structure of lizardite-1T from Elba, Italy. Am. Mineral. 79, 1194–1198.
Mellini, M., Fuchs, Y., Viti, C., Lemaire, C., Linairès, J., 2002. Insights into the antigorite structure from Mössbauer and FTIR spectroscopies. Eur. J. Mineral. 14, 97–104.
Metintas, M., Ak, G., Metintas, S., 2024. Environmetal asbestos exposure and lung cancer. Lung Cancer 194, 107850.

Mitchell, D.R., 2007. HRTEM Filter. Digital MicrographTM Scripting. http://www.dmscripting.com/hrtem_filter.html.
NIOSH, 2011. Asbestos Fibers and Other Elongate Mineral Particles: State of the Science and Roadmap for Research.
Oberdörster, G., Graham, U., 2018. Predicting EMP hazard: lessons from studies with inhaled fibrous and non-fibrous nano- and micro-particles. Toxicol. Appl. Pharmacol. 361, 50–61.
Ogniben, L., 1973. Schema Geologico della Calabria in base ai dati odierni. Geol. Romana 12, 243–585.
Oze, C., Solt, K., 2010. Biodurability of chrysotile and tremolite asbestos in simulated lung and gastric fluids. Am. Mineral. 95, 825–831.
Pacella, A., Ballirano, P., Fantauzzi, M., Rossi, A., Nardi, E., Capitani, G., Arrizza, L., Montereali, M.R., 2021. Surface and bulk modifications of amphibole asbestos in mimicked gamble's solution at acidic PH. Sci. Rep. 11.
Petriglieri, J.R., Laporte-Magoni, C., Salvioli-Mariani, E., Tomatis, M., Gazzano, E., Turci, F., Cavallo, A., Fubini, B., 2020. Identification and preliminary toxicological assessment of a non-regulated mineral fiber: fibrous antigorite from New Caledonia. In: Environ. Eng. Geosci. XXVI, pp. 89–97.
Petriglieri, J.R., Barale, L., Viti, C., Ballirano, P., Belluso, E., Bruno, M.R., Campopiano, A., Cannizzaro, A., Fantauzzi, M., Gianchiglia, F., Montereali, M.R., Nardi, E., Olori, A., Piana, F., Tomatis, M., Rossi, A., Skogby, H., Pacella, A., Turci, F., 2023. From field analysis to nanostructural investigation: a multidisciplinary approach to describe natural occurrence of asbestos in view of hazard assessment. J. Hazard. Mater. 457, 131754.
Prescher, C., McCammon, C., Dubrovinsky, L., 2012. MossA: a program for analyzing energy-domain Mössbauer spectra from conventional and synchrotron sources. J. Appl. Cryst. 45, 329–331.
Punturo, R., Bloise, A., Critelli, T., Catalano, M., Fazio, E., Apollaro, C., 2015. Environmental implications related to natural asbestos occurrences in the ophiolites of the Gimigliano-Mount Reventino Unit (Calabria, Southern Italy). Int. J. Environ. Res. Public Health 9 (2), 405–418.
Ross, M., Nolan, R.P., 2003. History of asbestos discovery and use and asbestos-related disease in context with the occurrence of asbestos within ophiolite complexes. In: Dilek, Y., Newcomb, S. (Eds.), Ophiolite Concept and the Evolution of Geological Thought, Boulder, Colorado, Geological Society of America, Special Paper, vol. 373, pp. 447–470.
Rossetti, F., Faccenna, C., Goffé, B., Funiciello, R., Monié, P., 2002. Tectono-metamorphic evolution of the high-P/low-T, ophiolite-bearing Gimigliano–Monte Reventino unit (Gimigliano, Sila Piccola). Insights for the tectonic evolution of the Calabrian Arc. Boll. Soc. Geol. Ital. 121, 51–69.
Rozalen, M., Ramos, M.E., Huertas, F.J., Fiore, S., Gervilla, F., 2013. Dissolution kinetics and biodurability of tremolite particles in mimicked lung fluids. Effect of citrate and oxalate. J. Asian Earth Sci. 77, 318–326.
Rozenson, I., Bauminger, E.R., Heller-Kallai, L., 1979. Moessbauer spectra of iron in 1:1 phyllosilicates. Am. Mineral. 64, 93–901.
Schott, J., Berner, R.A., 1983. X-ray photoelectron studies of the mechanisms of iron silicate dissolution during weathering. Geochim. Cosmochim. Acta 47, 2233–2240.
Stanton, M.F., Layard, M., Tegeris, A., Miller, E., May, M., Morgan, E., Smith, A., 1981. Relation of particle dimension to carcinogenicity in amphibole asbestos and other fibrous minerals. J. Natl. Cancer Inst. 67 (5), 965–975.
Turci, F., Tomatis, M., Lesci, I.G., Roveri, N., Fubini, B., 2011. The iron-related molecular toxicity mechanism of synthetic asbestos nanofibres: a model study for high-aspect-ratio nanoparticles. Chem. A Eur. J. 17, 50–358.
Turci, F., Favero-Longo, S.E., Gazzano, C., Tomatis, M., Gentile-Garofalo, L., Bergamini, M., 2016. Assessment of asbestos exposure during a simulate agricultural activity in the proximity of the former asbestos mine of Balangero, Italy. J. Hazard. Mater. 308, 321–327.
Uehara, S., 1998. TEM and XRD study of antigorite superstructures. Canad. Mineral. 36, 1595–1605.
Uehara, S., Shirozu, H., 1985. Variations in chemical composition and structural properties of antigorites. Mineral. J. 12, 299–318.
Utembe, W., Potgieter, K., Stefaniak, A.B., Gulumian, M., 2015. Dissolution and biodurability: important parameters needed for risk assessment of nanomaterials. Part. Fibre Toxicol. 12, 11.
Vignaroli, G., Ballirano, P., Belardi, G., Rossetti, F., 2014. Asbestos fibre identification vs. evaluation of asbestos hazard in ophiolitic rock melanges, a case study from the Ligurian Alps (Italy). Environ. Earth Sci. 72 (9), 3679–3698.
Virta, R., 2006. Worldwide asbestos supply and consumption trends from 1900 through 2003. In: U.S. Geological Survery Circular 1298 (80 pp.).
Vitale, S., Ciarcia, S., Fedele, L., Tramparulo, F., 2019. The Ligurian oceanic successions in southern Italy: the key to decrypting the first orogenic stages of the Southern Apennines-Calabria chain system. Tectonophysics 750, 243–261.
Weill, D., 2018. Proceedings of the Monticello conference on elongate mineral particles (EMP). Toxicol. Appl. Pharmacol. 361, 1–2.
WHO, 1997. Determination of airborne fibre number concentrations. In: A Recommended Method, by Phase-Contrast Optical Microscopy (Membrane Filter Method)., Geneva, 1997 (https://doi.org/ISBN9241544961).
Wicks, F.J., O'Hanley, D.S., 1988. Serpentine minerals: structures and petrology. In: Bailey, S.W. (Ed.), Hydrous Phyllosilicates (Exclusive of Micas). Rev. Mineral, vol. 19 (91167).
Wylie, A.G., Korchevskiy, A.A., 2023. Dimensions of elongate mineral particles and cancer: a review. Environ. Res. 230.